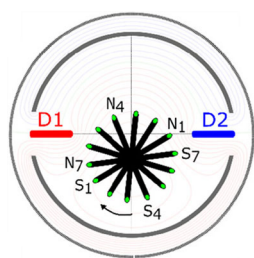RESEARCH ARTICLE

Cyclotron Phase-Coherent Ion Spatial Dispersion in a Non-Quadratic Trapping Potential is Responsible for FT-ICR MS at the Cyclotron Frequency

Konstantin O. Nagornov, Anton N. Kozhinov, Yury O. Tsybin

Spectroswiss, EPFL Innovation Park, 1015, Lausanne, Switzerland

Abstract. Fourier transform ion cyclotron resonance mass spectrometry (FT-ICR MS) at the cyclotron frequency instead of the reduced cyclotron frequency has been experimentally demonstrated using narrow aperture detection electrode (NADEL) ICR cells. Here, based on the results of SIMION simulations, we provide the initial mechanistic insights into the cyclotron frequency regime generation in FT-ICR MS. The reason for cyclotron frequency regime is found to be a new type of a collective motion of ions with a certain dispersion in the initial characteristics, such as pre-excitation ion velocities, in a highly non-quadratic trapping potential as realized in NADEL ICR cells. During ion detection, ions of the same m/z move in phase for cyclotron ion motion but out of phase for magnetron (drift) ion motion destroying signals at the fundamental and high order harmonics that comprise reduced cyclotron frequency components. After an initial magnetron motion period, ion clouds distribute into a novel type of structures – ion slabs, elliptical cylinders, or star-like structures. These structures rotate at the Larmor (half-cyclotron) frequency on a plane orthogonal to the magnetic field, inducing signals at the true cyclotron frequency on each of the narrow aperture detection electrodes. To eliminate the reduced cyclotron frequency peak upon dipolar ion detection, a number of slabs or elliptical cylinders organizing a star-like configuration are formed. In a NADEL ICR cell with quadrupolar ion detection, a single slab or an elliptical cylinder is sufficient to minimize the intensity of the reduced cyclotron frequency components, particularly the second harmonic.

Keywords: Fourier transform, FT, Fourier transform mass spectrometry, FTMS, Ion cyclotron resonance, ICR, Ion motion, Cyclotron frequency, Magnetron frequency, Reduced cyclotron frequency

Introduction

Ion motion in a mass analyzer (cell) of a Fourier transform ion cyclotron resonance mass spectrometer (FT-ICR MS) is typically described by the three components of ion motion with their corresponding frequencies: the reduced cyclotron motion and frequency, ω_+, the magnetron motion and frequency, ω_-, and the axial oscillations motion and frequency, ω_z [1, 2]. Jointly, the ω_+ and ω_- ion motion components and frequencies describe two types of ion motion in an ICR cell that have usually been employed in practice to date. The first, and by far the most common one, is organized when each group of ions of the same m/z values is bunched into a cloud that rotates as a whole at the excited cyclotron radius [1, 2]. According to the modern understanding of the FT-ICR MS, this ion cloud is a result of a 2D projection from a cigar-shaped cylinder aligned with the magnetic field axis [3]. The associated magnetron radii of these rotating ion clouds (or cylinders) are much smaller than their cyclotron radii. As a result, the typically employed dipolar ion detection yields ion signals at the reduced cyclotron frequency, ω_+, which is a cyclotron frequency shifted down by the radial component of the trapping electric field by the value of the magnetron frequency: $\omega_+ = \omega_c - \omega_-$ [1]. Owing to a direct dependence of the magnetron frequency on the trapping potential, the reduced cyclotron frequency shows a pronounced dependence on trapping voltages and space charge field [4, 5]. The second, and very rarely employed, type of ion motion is realized when the radius of magnetron motion of an ion cloud is close to or greater than the cyclotron

Correspondence to: Yury O. Tsybin; e-mail: tsybin@spectroswiss.ch

motion radius. The limited practical utility of this type of ion motion was put forward via its use for a direct measurement of the cyclotron frequency using quadrupolar ion detection arrangements [6–8]. For this type of ion motion, groups of ions of the same m/z are believed to be bunched in the rotating clouds (cylinders), similar to the first type of ion motion. Therefore, both magnetron and cyclotron motions for all ions in each cloud are in phase for both types of ion motion known today.

A theoretical independence of the unperturbed or true cyclotron frequency from applied trapping potentials and space charge fields was historically suggested as an advantage over the reduced cyclotron frequency detection for precision mass spectrometry [9–11]. However, the practical implementation of an ICR cell with quadrupolar ion detection, uniquely enabling ion detection at the unperturbed cyclotron frequency allowed mass measurement of ions only from atoms, e.g., argon, and small molecules. Indeed, the observed cyclotron frequency peak was always accompanied by a pronounced second harmonic of the reduced cyclotron frequency, $2\omega_+$, which is undesirable for practical applications of FT-ICR MS. In addition, mass measurements of large (bio)molecules at the cyclotron frequency were not accomplished with the ICR cells employed in those studies. Therefore, enabling FT-ICR MS operation at the unperturbed cyclotron frequency for large molecules and in the absence of harmonic peaks would be welcome. It may reduce a negative influence of space charge fields on mass measurement accuracy, thus facilitating mass spectra calibration [4, 5, 12–14]. The latter could be particularly useful in experiments with fluctuating ion sources, such as in imaging mass spectrometry and in on-line separations-based FT-ICR MS [15]. Furthermore, reduced independence on the trapping potential may enable ICR cell operation (including ion detection) at elevated (10–100 V) potentials, reducing ion leakage from the cell upon energetic in-cell ion fragmentation events, for example electron capture and electron ionization dissociation [16–19].

Recently, we reported on the first experimental implementation of FT-ICR MS at the cyclotron frequency instead of the reduced cyclotron frequency for both small and large (bio)molecules [20]. Briefly, during experimental characterization of narrow aperture detection electrodes (NADEL) ICR cell with dipolar ion excitation and detection our group has observed an efficient generation of peaks at the cyclotron frequency and an almost complete suppression of peaks at the reduced cyclotron frequency. We found this regime to be characterized by the following features [20]: (1) the reduced cyclotron frequency peak can be efficiently (completely) converted into the cyclotron frequency peak by a slight, on the order of 100 mV, variation in the offset DC potentials applied to the excitation electrodes; (2) the (observed) cyclotron frequency is nearly independent of the trapping electric field; (3) the (observed) cyclotron frequency depends significantly weaker on the number of charges injected into the ICR cell than in the reduced cyclotron frequency regime realized with the same ICR cell; (4) the sensitivity performance in the unperturbed cyclotron frequency regime can be made comparable to that in the standard reduced cyclotron frequency regime

when both regimes are realized in the same experimental setup; (5) transients in the cyclotron frequency regime have a characteristic initiation period of up to 100–200 ms for standard experimental conditions during which signal intensity drops almost to the noise level and then restores; the duration of this initiation period shortens with an increase in trapping potential.

In an attempt to improve the analytical characteristics of the initial implementation of FT-ICR MS at the cyclotron frequency, we implemented the next generation of the NADEL ICR cells, which enabled quadrupolar ion detection via addition of another pair of flat detection electrodes and splitting each of the original excitation electrodes into two [21]. The observed characteristics demonstrated improved performance compared with the NADEL ICR cell with dipolar ion detection, including even better independence from trapping potentials and simplified parameter optimization (no offset potentials required). The characteristic initiation period visible in the first ~100 ms of a transient remained. As expected, mass spectra contained peaks at both cyclotron and double reduced cyclotron frequencies [8]. However, parameter optimization allowed us to significantly reduce the $2\omega_+$ harmonic. Therefore, whereas a certain resemblance was observed between those results and the work of Schweikhard and co-workers [8], pronounced differences were indicating a novel FT-ICR MS regime with quadrupolar ion detection. Experimental observation of the cyclotron frequency generated by a dipolar ion detection arrangement was even more puzzling and unexpected.

To rationalize the observed cyclotron frequency regimes in FT-ICR MS with both dipolar and quadrupolar ion detection, we have performed extensive SIMION simulations, the first results of which are reported here. The key to the mechanism of the cyclotron frequency generation was found to be the development of a principally new, third type of ion cloud formation and collective motion in the ICR cell. Contrary to the two ion motion types described above, here ions of even the same m/z values are spatially distributed in the volume of the ICR cell, keeping only their cyclotron motions in phase, but allowing for their magnetron motions to be out of phase. Thus, ion frequency peaks that contain the magnetron (drift) frequency component, namely the reduced cyclotron frequency peaks for dipolar ion detection and the $2\omega_+$ peaks for quadrupolar ion detection, are destroyed by the many ions of the same m/z employed for ion detection in a typical ICR experiment.

Experimental

SIMION Simulations

Simulations of ion motion and transient generation were performed to model the working conditions of an FT-ICR mass spectrometer equipped with a 10 T superconducting magnet and diverse ICR cells. Particularly, the ICR cell geometries close to those of Ultra (Thermo Scientific, Bremen, Germany) and NADEL (Spectroswiss, Lausanne, Switzerland) ICR cells were modeled using the SIMION 3D software (ver. 8.1, Idaho National Engineering and Environmental Laboratory, Idaho Falls, ID,

USA) with a grid step of 0.2 mm. The Ultra ICR cell geometry represented a cylindrical surface with the two 90° wide excitation electrodes and two 90° wide detection electrodes, as described previously [22]. Both Ultra and NADEL ICR cells had an aspect ratio of 2.5 (a length of 140 mm and an inner diameter of 56 mm). The NADEL ICR cell configurations corresponded to the experimental studies for dipolar ion detection (two flat detection electrodes and a pair of ~180° wide excitation electrodes) and for quadrupolar ion detection (four flat detection electrodes and two pairs of ~90° wide excitation electrodes), Figure 1 [21, 23]. The grids employed in the experimental work for ion excitation in both Ultra and NADEL ICR cells were not taken into consideration for the simulated geometries. Correspondingly, the trapping rings were not segmented, contrary to the trapping electrodes ensemble in the experimental cells. The modeled geometries were superimposed with the SIMION simulated 10 T homogeneous magnetic fields in the whole volume of the cells, similar to the prior work of Hendrickson and co-workers [24]. The 10 T field corresponded to the experimental conditions in the original work.

The magnetic field comes up out of the plane perpendicular to the magnetic field axis for all figures reported here.

The following experimental sequences and parameters were employed for each in-silico calculation. For the first group of calculations, a positive ion or a group of positive ions (at 524 m/z) were generated in the region of the grounded front trapping ring electrode with the defined initial parameters, Figure 1. An ion position was given by x, y, z coordinates and an ion velocity was given by axial velocity, V_z, directed to the center of the ICR cell, with the corresponding parameter spread for a group of ions. Ion initial radial velocities, V_x and V_y, were set to 0 for all calculations. Initial parameters were preset randomly in the specified range of parameters for a group of ions or manually for a single ion. The same trapping potential of 2.5 V or 5 V was kept on the rear trapping ring electrode for all events, including ion excitation and detection. At the initial moment of time, a DC voltage of –6 V or –15 V was applied to the front trapping ring electrode. When injected ion or ion cloud (cylinder) reached the center of the ICR cell, the $z = 70$ mm plane, the front trapping ring electrode potential
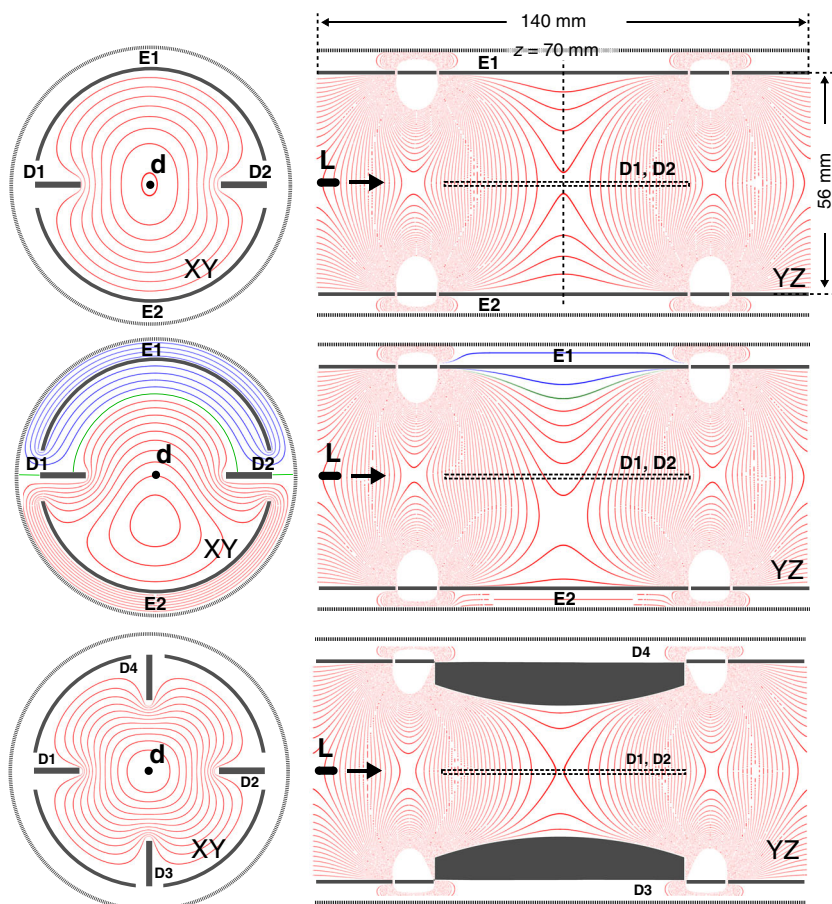
Figure 1. Geometry of SIMION-simulated NADEL ICR cells. The trapping potential distributions of a NADEL ICR cell with two detection and excitation electrodes are shown for the following parameters: (Top panel) V_{trap} = 5 V, V_{E1} = V_{E2} = 0 mV, and (middle panel) V_{trap} = 5 V, V_{E1} = –90 mV, V_{E2} = 150 mV. (Bottom panel) the trapping potential distribution of a NADEL ICR cell with four detection and excitation electrodes calculated with V_{trap} = 5 V, V_{E1} = V_{E2} = 0 mV. Ions were generated with random or predefined coordinate values x, y, and z in the cylinder region with diameter d and length L. E1, E2, E3, and E4 indicate the excitation electrodes; D1, D2, D3, and D4 – narrow aperture detection electrodes. Equipotential contours are from –0.08 to 0.20 V with a step of 0.02 V for the XY plane; –0.04 to 2.04 V with a step of 0.04 V for the YZ plane

was changed to match the potential of the rear trapping ring electrode, thus simulating a gated ion trapping. For the second group of calculations, each ion was placed on-axis directly in the center $z = 70$ mm of the ICR cells. Ion initial velocity distributions were thus assigned to the in-cell located ions prior to ion excitation.

Following a delay of 1 ms after ion placement on the ICR cell axis in either of the approaches described above (external or internal ion placement), ions were excited by a sweep dipolar excitation (289–295 kHz) applied to the excitation electrodes during 100 us. Importantly, to ensure a proper excitation simulation, SIMION code was updated following earlier recommendations by Wilcox et al. [25]. For the NADEL ICR cell with two excitation electrodes, a conventional dipolar ion excitation was simulated, whereas for the NADEL ICR cell with four excitation electrodes, after a dipolar ion excitation an additional DC sidekick pulse of ±17 V was applied for 100–300 us to the opposite excitation electrodes to shift the ion population off-axis (to increase magnetron radius). The latter was necessary due to the symmetry of the trapping potential around the center of the cell in the NADEL ICR cell with four excitation electrodes.

Similar to the real-life experiment, intensities of sidebands and peak shapes in SIMION simulations of the NADEL ICR cell with a single pair of detection and a single pair of excitation electrodes were optimized via independent variation of the four offset DC potentials V_{E1}, V_{E2}, V_{D1}, and V_{D2} applied to the excitation electrodes E1 and E2, and detection electrodes D1 and D2, respectively, throughout the entire experimental sequence, Figure 1 middle panel. The offset DC potentials were set to values between −150 and 150 mV with a step of 1 mV for the positive and negative ion modes, independently, unless stated otherwise. Simulations show that even such a relatively low offset DC potential significantly disturbs the trapping potential, especially close to the center of the cell at $z = 70$ mm, Figure 1 middle panel. However, the influence is not so strong for the cell region close to the trapping rings where the trapping electric field is much stronger. Owing to a narrow aperture of the detection electrodes, their offset DC potentials V_{D1} and V_{D2} were set equal to zero.

Importantly, Figure 1 clearly demonstrates a significant deviation of the trapping potential in the NADEL ICR cells from the quadratic trapping potential employed in the conventional ICR cells for detection of the reduced cyclotron frequency. Indeed, trapping potential in ion motion volumes of (cylindrical) ICR cells typically employed for FT-ICR MS is close to quadratic and can be approximated by $U(r,z) = -C \cdot \left(\frac{r^2}{2} - z^2 \right)$ and, ideally, it does not depend on the azimuthal coordinate. On the plane orthogonal to the magnetic field and at the cell center, this trapping potential corresponds to a linear radial trapping field. Instead, trapping electric field created in the NADEL ICR cells is characterized by a significant azimuthal dependence of the trapping potential. Equipotential field lines take the form of ellipses and super-ellipses, indicating a radical departure from the ideal circles in the conventional modern FT-ICR MS, Figure 1. In fact, these trapping potentials resemble the trapping potentials created in the (now historic)

cubic ICR cells and in the elliptical ICR cells developed for FT-ICR MS applications in basic research [2, 26]. In this work, we refer to the fields and their corresponding potentials created in the NADEL ICR cells as non-linear trapping fields and non-quadratic trapping potentials.

The current induced in the detection circuitry by ions flying during a certain period of time, for example 1 s, inside an ICR cell and taking into account ion axial motion was computed with the digitization (sampling) frequency of 2 MHz, unless stated otherwise, by using the approach based on the Shockley-Ramo theorem as implemented in SIMION [24]. For dipolar ion detection, the time-domain signals (transients) were produced by subtraction of signals acquired with two detection electrodes from one another. For quadrupolar ion detection, the time-domain signals (transients) were produced by subtraction of the two signals, each obtained by summation of signals from the opposite detection electrodes. SIMION simulated transients were apodized with the Hann window, zero-filled twice (in recursive terms), and Fourier transformed (FT). The peaks were picked using three-point parabolic interpolation. Signal processing and data visualization were performed using the Peak-by-Peak data processing and analysis framework (Spectroswiss).

Results and Discussion

Dipolar Ion Detection: Frequency Conversion for a Single Ion

Figure 2 shows an influence of the trapping potential on ion trajectories, corresponding transients, and frequency spectra composition for the simulated NADEL ICR cell with dipolar ion excitation and detection. Shown are the trapping potential distributions onto the XY plane at $z = 70$ mm and projections of ion trajectories on the XY planes in the whole volume of an ICR cell during the 1 s detection time. A redistribution of signal intensity between the reduced cyclotron frequency and cyclotron frequencies in the frequency spectra as a function of offset DC potentials for a single ion and a group of 500 ions is clearly observed and is discussed below.

First, the time-domain signal was generated with a single ion flying in the NADEL ICR cell (initial, close to a realistic ion velocity $V_z = 0.86$ mm/us (~2.15 eV); initial ion coordinates $x, y = 0$ mm and $z = 1$ mm) at the trapping potential of $V_{trap} = 2.5$ V and offset DC potentials of $V_{E1} = 0$ mV and $V_{E2} = 0$ mV. In this case, the trajectory of ion motion is a circle with a given constant radius and the rotation axis in the geometric center of the cell, Figure 2a. A Fourier spectrum of the calculated transient has a dominant peak at 293048.3 Hz, which corresponds to the reduced cyclotron frequency for selected trapping potential, as expected. Theoretical value of the cyclotron frequency for 524 m/z ion at the same experimental conditions would be 7.4 Hz higher and equal to 293,055.7 Hz. Despite the fact that the trapping potential
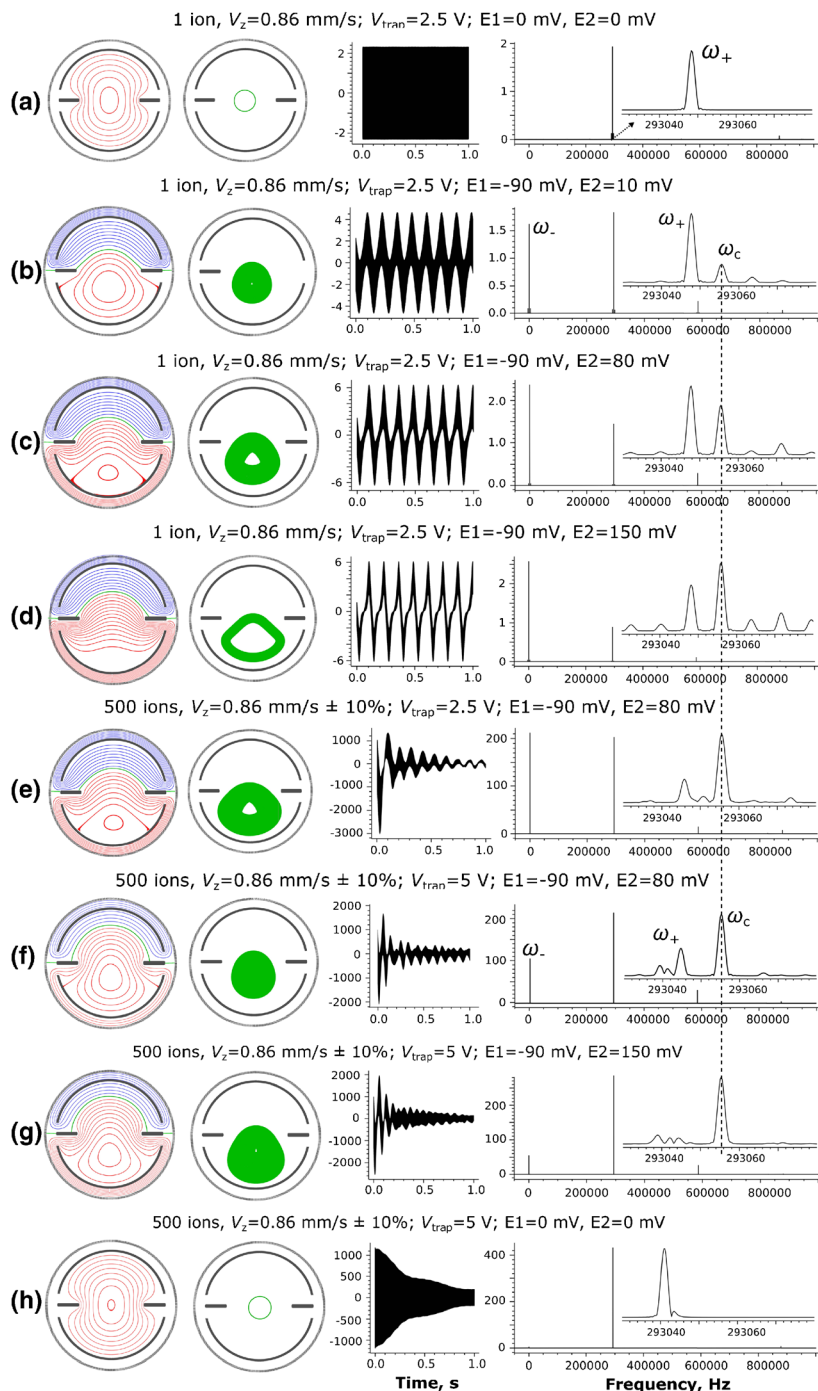
Figure 2. SIMION-generated relationships between trapping potential distributions, ion trajectories, transients, and frequency (mass) spectra demonstrating 524 m/z ion detection in the NADEL ICR cell. (First column) shows trapping potential distribution with diverse offset DC potentials V_{E1} and V_{E2} being taken into account. The equipotential contours of (blue line) negative, (red line) positive, and (green line) zero potentials at $z = 70$ mm are indicated with the increment or decrease of 0.1 V for calculations with $V_{trap} = 2.5$ and of 0.2 V for calculations with $V_{trap} = 5$. (Second column) shows the corresponding ion trajectories on the XY plane perpendicular to the magnetic field at $z = 70$ mm. (Third column) shows the subsequently obtained transients. (Fourth column) shows the corresponding frequency spectra after Fourier transformation. Peaks shown for frequency spectra correspond to the reduced cyclotron frequency, ω_+, the magnetron (drift) frequency, ω_-, the cyclotron frequency, ω_c, and the axial oscillations frequency, ω_z. Initial ion parameters for calculations with groups of ions were set randomly with Gaussian distributions: initial ion velocity in the axial direction to the center of the cell $V_{z, mean} = 0.86$ mm/us and $V_{z, std. dev.} = 0.08$ mm/us; a cylinder for ion spatial distribution in the axial direction had a length of 1.5 mm and diameter of 0.8 mm. Simulations parameters for each case are shown above the corresponding frequency spectra

distribution was elliptical in the center of the cell, the cyclotron orbit was not distorted noticeably. Nevertheless, the sidebands corresponding to the double frequency of the axial ion motion were present around the dominant peak, $2*f_{\text{axial}} = 1962.3$ Hz, Figure 2a.

The equipotentials of the trapping electric field were significantly shifted with the application of the asymmetric offset DC potentials, $V_{\text{E1}} = –90$ mV and $V_{\text{E2}} = 10$ mV, Figure 2b. As expected, an ion follows the equipotential lines (magnetron or low-frequency drift motion) while performing cyclotron cycles of ion rotation, Figure 2b. Oscillations at the magnetron frequency became visible in the transient, Figure 2b. For this ion trajectory, additional magnetron sidebands appeared around the dominant reduced cyclotron frequency signals in the frequency spectra, including a sideband at 293,055.6 Hz corresponding to the cyclotron sideband frequency, denoted here as ω_{c}, and another peak in the low frequency range corresponding to the magnetron frequency, ω_{-}.

The intensity of ω_{c} w.r.t. ω_{+} peak increased with an increase of the difference between offset DC potentials applied to the opposite excitation electrodes, as the radius of a magnetron orbit, $R_{\text{magnetron}}$, increases relative to the cyclotron orbit, $R_{\text{cyclotron}}$, Figure 2c. Notably, at these conditions, the intensity of the ω_{c} peak became comparable with the intensity of the ω_{+} peak for a single ion detection. Further increase of the offset DC potentials difference increased the intensity of all harmonics. However, the intensity of the ω_{c} peak remained comparable with the intensity of the ω_{+} peak even with an increase of the ratio $R_{\text{magnetron}}/R_{\text{cyclotron}}$ via decreasing the cyclotron radius, Figure 2d. Therefore, according to the SIMION simulations, the cyclotron frequency regime observed in the FT-ICR MS experiment with a given configuration of a NADEL ICR cell, where ω_{c} peak is dominant and intensity of harmonics (sidebands) are less than 5% (which corresponds to the real-life experiment), cannot be realized with a single ion, at least at the typical ion detection periods. Nevertheless, these results suggest that an efficient, up to 50%, conversion of the reduced cyclotron frequency peak intensity into the cyclotron peak may take place in the highly non-linear electric fields for the current experimental geometry and accuracy of SIMION simulations.

Dipolar Ion Detection: Cyclotron Frequency Generation from Many Ions

To obtain a better correlation between simulated and experimental data, we simulated detection of a group of 500 ions having a spread of initial parameters but flying simultaneously inside the NADEL ICR cell at the trapping potential of $V_{\text{trap}} = 2.5$ V and offset DC potentials of $V_{\text{E1}} = –90$ mV and $V_{\text{E2}} = 80$ mV, Figure 2e. The resultant frequency spectrum from 500 ions demonstrates that intensity of the ω_{+} peak and the magnetron sidebands, as well as of the ω_{-} peak, are abruptly

decreased w.r.t. the intensity of the ω_{c} peak compared with the calculations with a single ion and the same experimental parameters. The intensities of sidebands attributable to the axial oscillations were also decreased noticeably. Indeed, the amplitude and the frequency of axial ion motion depend on the initial ion velocity for an open-ended cylindrical ICR cell [1, 27]. The ion cloud with the initial ions' velocity spread is stretched in the axial direction of the cell already during several ion axial oscillations, as will be shown below, so that the axial frequency of ion motion cannot be detected. However, the intensities of magnetron sidebands were still higher than 30% w.r.t. the intensity of the ω_{c} peak. Note, the intensities of parasitic peaks in ω_{c} regime were also higher for low trapping potentials in the experimental studies [20].

To verify the lack of a frequency shift for the ω_{c} peak as a function of trapping potential, we generated SIMION data with 500 ions with the same offset DC potentials of $V_{\text{E1}} = –90$ mV and $V_{\text{E2}} = 80$ mV with a spread in the initial parameters as in the previous calculation but with the twice increased trapping potential, $V_{\text{trap}} = 5$ V, Figure 2f. The frequency shift was not observed for the cyclotron frequency peak, ω_{c}, but it was observed for the reduced cyclotron frequency peak, ω_{+}, as expected. Nevertheless, the intensity of the ω_{+} peak was increased w.r.t. the intensity of ω_{c} peak compared with the previous calculation with a lower trapping potential and the same offset DC potentials. The trapping field distribution demonstrates that owing to the higher trapping potential, the electric field axis moved closer to the geometric center of the cell. Correspondingly, the trajectory projection of ions demonstrates a much smaller radius of the magnetron orbit, Figure 2f. In accordance with the experimental results, the intensity of the ω_{+} peak was significantly decreased, to less than 15% w.r.t. ω_{c} peak, with an increase of a difference between the offset DC potentials to the values of $V_{\text{E1}} = –90$ mV and $V_{\text{E2}} = 150$ mV at the same trapping potential of 5 V, Figure 2g. The radius of magnetron orbit was increased, as expected. Note the presence of high order harmonics, $2\omega_{+}$ and $3\omega_{+}$, in the frequency spectra, Figure 2.

Finally, the standard reduced cyclotron frequency regime, where axes of cyclotron orbit, electric field, and the cell geometric center all match each other, was simulated using the randomly generated 500 ions, detection period of 1 s and $V_{\text{trap}} = 5$ V without the DC offset application, Figure 2h. As expected, the corresponding frequency spectrum demonstrates the symmetrical peak shape of the dominant ω_{+} peak, with the resolution close to the theoretical one. However, the decaying time-domain signal reflects the phase de-coherence of the ion cloud, Figure 2h. The latter is an expected result for a high trapping potential of 5 V in the reduced cyclotron frequency regime, especially in the employed here non-quadratic trapping potential.

To summarize, simulation results suggest that a superposition of the magnetron (drift) and cyclotron motions of a group of ions with a spread in their axial ion velocities could be the reason of the cyclotron frequency, ω_c, regime. The region around the ω_+ peak in the frequency spectrum for calculations with many ions contained not one, as for the single ion calculation, but a number of peaks. Under the realistic experimental conditions, the noise from the detection circuitry may cover these remainders of the destroyed reduced cyclotron frequency peak [20]. On the contrary, the region around the ω_c peak contained a single peak for both calculations with a single and many ions; an increase in its magnitude is observed for the case of many ions compared with the single ion case.

Cyclotron Frequency Generation: Effect of Initial Parameters

Why does the ω_c peak start to significantly dominate other peaks, including ω_+, $2\omega_+$, and ω_- harmonics, in a NADEL ICR cell with the application of offset potentials? To address this question, transients and frequency spectra were generated with the ICR cell parameters $V_{E1} = -90$ mV, $V_{E2} = 150$ mV, and $V_{trap} = 5$ V for a single ion, two ions, 32 ions, 280 ions, and 560 ions, Figure 3. Ions were generated with the preset initial velocity $V_z = 0.82$ mm/us $+ \Delta V_z$ and initial coordinates x, y, and z. The initial parameters were changed one by one for each separate calculation with the following steps: $z = 1$ mm or 3 mm; $\Delta V_z = 0.00025*n$ mm/us, where $n = 0...279$. Each ion had the trajectory in each calculation as shown in Figure 2g. The corresponding frequency spectra are characterized by the ω_-, ω_+, and ω_c peaks being dominant in the presence of other, less intensive inter-harmonics, Figure 3a.

The simulations show that the reduced cyclotron frequency, ω_+, and the corresponding magnetron frequency, ω_-, depend on the initial ion velocity V_z. Specifically, the ω_+ frequency decreases and the ω_- increases with an increase of ion velocity, Figure 3a and b. On the other hand, the cyclotron frequency, ω_c, was almost independent of the ion velocity. As a result, the intensities of all inter-harmonics, as well as the ω_- peak intensity, decrease w.r.t. the ω_c peak with the summation of transients generated by ions
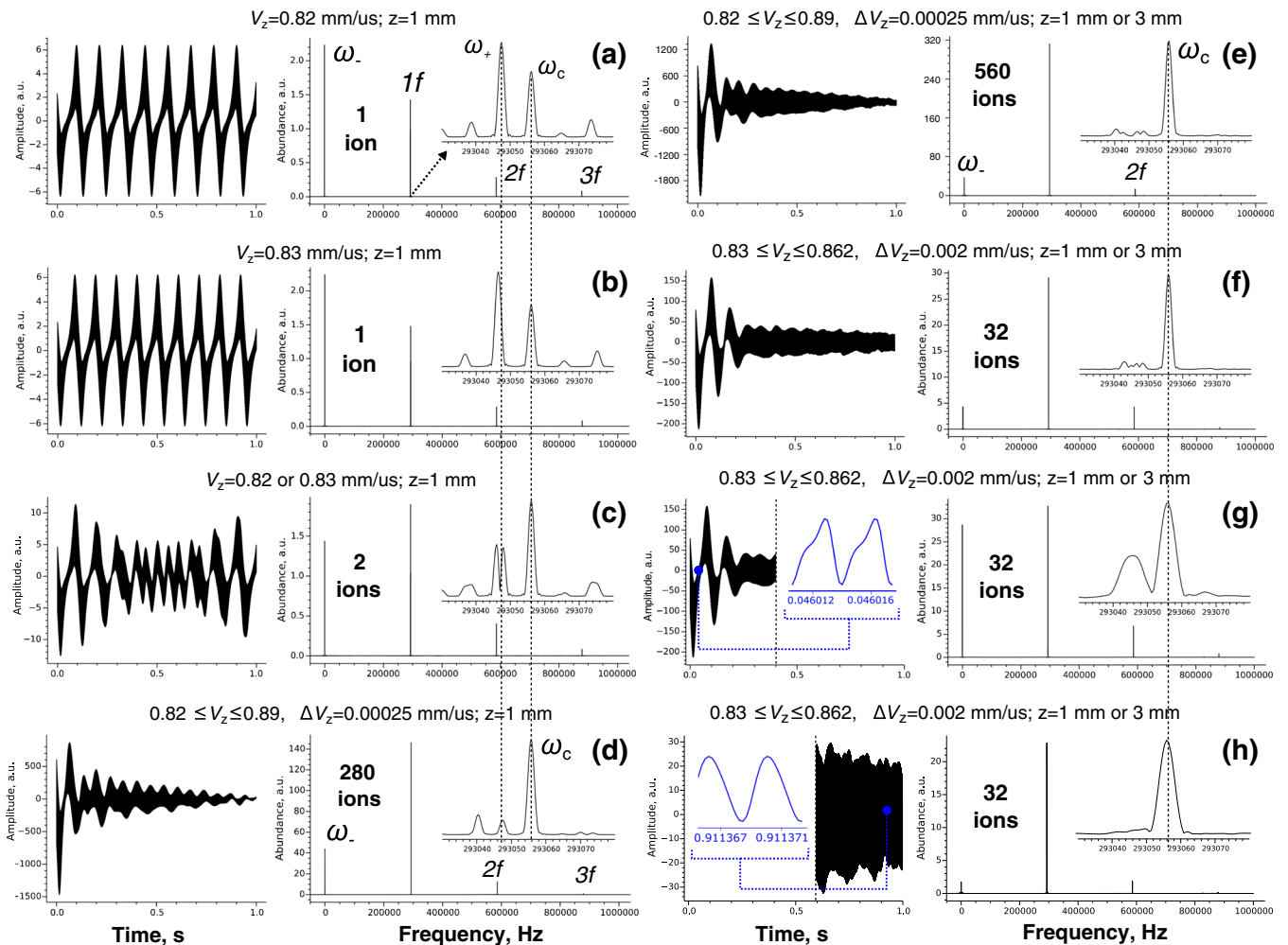

Figure 3. SIMION-simulated time-domain signals (transients) and the corresponding frequency spectra generated by a single ion or groups of ions with different initial parameters moving in the NADEL ICR cell. The following parameters were employed: $V_{trap} = 5$ V, $V_{E1} = -90$ mV, and $V_{E2} = 150$ mV. Each ion was created with an initial ion velocity V_z and z position: $V_z = 0.82000 + 0.00025*n$ mm/us, where $n = 0...279$; $z = 1$ mm or 3 mm on axis ($x = y = 0$mm); 560 parameter combinations in total. Notations are as in Figure 2

with different initial ion velocities V_z, Figure 3c and d. The higher spread of ion velocity V_z and higher number of ions in a group provided less intense parasitic harmonics and inter-harmonics in a final frequency spectrum in the cyclotron frequency regime, including the most intensive "parasitic" peaks ω_+, $2\omega_+$, $3\omega_c$, *etc.*

Additionally, slight deviation of the reduced cyclotron frequency, ω_+, and the invariance of the ω_c frequency peak were observed with a variation of the initial ion axial, z, position. A similar effect for the reduced cyclotron frequency was observed with SIMION calculations and discussed by Luebkemann and co-workers [28]. The summation of the transients generated by ions with the same velocities but started from different z position on the axis increases the domination of the ω_c peak in the final frequency spectrum, Figure 3e, and Figure S1A, C, and E (Supplementary Information). Correspondingly, the deviation of the reduced cyclotron frequency, ω_+, was orders of magnitude smaller depending on initial x or y position of ion within 1 mm away from the geometric axis. The ratio of peak relative intensities in the frequency spectrum of the sum of four transients generated by ions with the same V_z and z, but with different x and y parameters remained almost unchanged compared with the single ion calculation with the same V_z and z, Figure S1A and B (Supplementary Information). The initial spatial distribution within a 2-mm diameter spot of an ion cloud in the plane perpendicular to the magnetic field did not significantly affect the final spectral composition.

Importantly, already 32 ions with diverse initial parameters V_z and z were enough to get the typical for the ω_c regime spectral composition observed in the experiment, Figure 3f. Nonetheless, the relatively high intensity of parasitic peaks w.r.t. the ω_c peak is observed. On the other hand, owing to a noise band of modern data acquisition electronics in FTMS being at the level of 3–5 charges and to a potentially larger dispersion of ion initial velocities and coordinates in a real-life experiment, the required number of ions for establishing the cyclotron frequency regime would match the typical experimental conditions for many applications. Moreover, longer ion detection would further contribute to the disappearance of the reduced cyclotron frequency ω_+ component because of increased resolution and thus lower interference of the contribution to this component from all ions. That is similar to the peak splitting and intensity decrease in isotopic fine structure observation at a higher resolution compared with the standard ^{13}C isotopic envelope for peptides detected with a lower resolution.

Transient Signal Structure in the Cyclotron Frequency Regime

A particular structure of the transient signal has been reported for the cyclotron frequency regime [20]. Specifically, transients exhibit a strong decaying behavior for the initial period of 100–200 ms, which correlates with the simulations described above. Simulations demonstrate that a Fourier spectrum of the initial transient

segment reveals a pronounced reduced cyclotron frequency peak in the spectral composition, Figure 3g and h. On the other hand, FT of the subsequent post-initial segment of the transient yields a practically cyclotron frequency-only spectrum. Transient decay in the initial segment is related to the stretching of an ion ensemble along the magnetron (drift) orbit. In other words, the decay is caused by an increase of the magnetron frequency phase shift difference of separate ions due to different values of the pre-excitation ion velocity V_z or initial coordinate z, Figure S1 (Supplementary Information). As a result, the intensity of the magnetron frequency component becomes significantly reduced at the moment when the separate cyclotron oscillators spread out on the magnetron orbit and close the ring, see Figure 4 below. Thereby, the intensity of the magnetron frequency peak ω_- is significantly lower in the frequency spectrum corresponding to the post-initiation period of a transient compared to the frequency spectrum obtained from the initial part of the same transient, as confirmed by Figure 3g and h. Similar difference of intensity behavior of the ω_+ peak is observed for the frequency spectra from the initial and the post-initial segments of a transient.

The difference of a phase shift of the reduced cyclotron frequency ω_+ of separate ions increases with time similar to the magnetron frequency phase shift, as these two frequencies depend on each other, Figure S2 (Supplementary Information). The intensity of the ω_c peak reduces as well when the two transient segments are compared, Figure 3g and h. However, this reduction is an order of magnitude smaller compared to the ω_+ and ω_- peaks because of the much smaller phase shift difference for cyclotron frequency, Figure S2 (Supplementary Information). The finite phase shift difference for the ω_c frequency suggests that the measured (simulated) quantity ω_c for a given experimental configuration approximates the cyclotron frequency, although the experimental (simulated) frequency is not equal exactly to the theoretical cyclotron frequency. Additionally, Figure S2 (Supplementary Information) shows that the difference of the phase shift for all three main frequencies increases with an increase of the spread of ion velocity for the group of ions (left panel versus right panel). Henceforth, the transient decays faster for a group of ions with a wider ion velocity spread, Figure 3e and f.

Ion Motion in a NADEL ICR Cell with a Dipolar Ion Excitation and Detection

The trajectories of ion motion for 280 ions in the NADEL ICR cell were investigated in detail during the calculation period of 1 s with the experimental parameters employed in Figure 3d. The coordinates x, y, and z were recorded for each ion with a sampling frequency of 5 MHz. It allowed us to visualize a spatial distribution of ions inside the ICR cell for each recorded time step of 0.2 ns (or $2\pi/17$ of a cyclotron cycle for a singly charged 524 m/z ion in a 10 T magnetic field), Figure 4. Snapshots of the 2D projections of ion trajectories from the whole volume of the
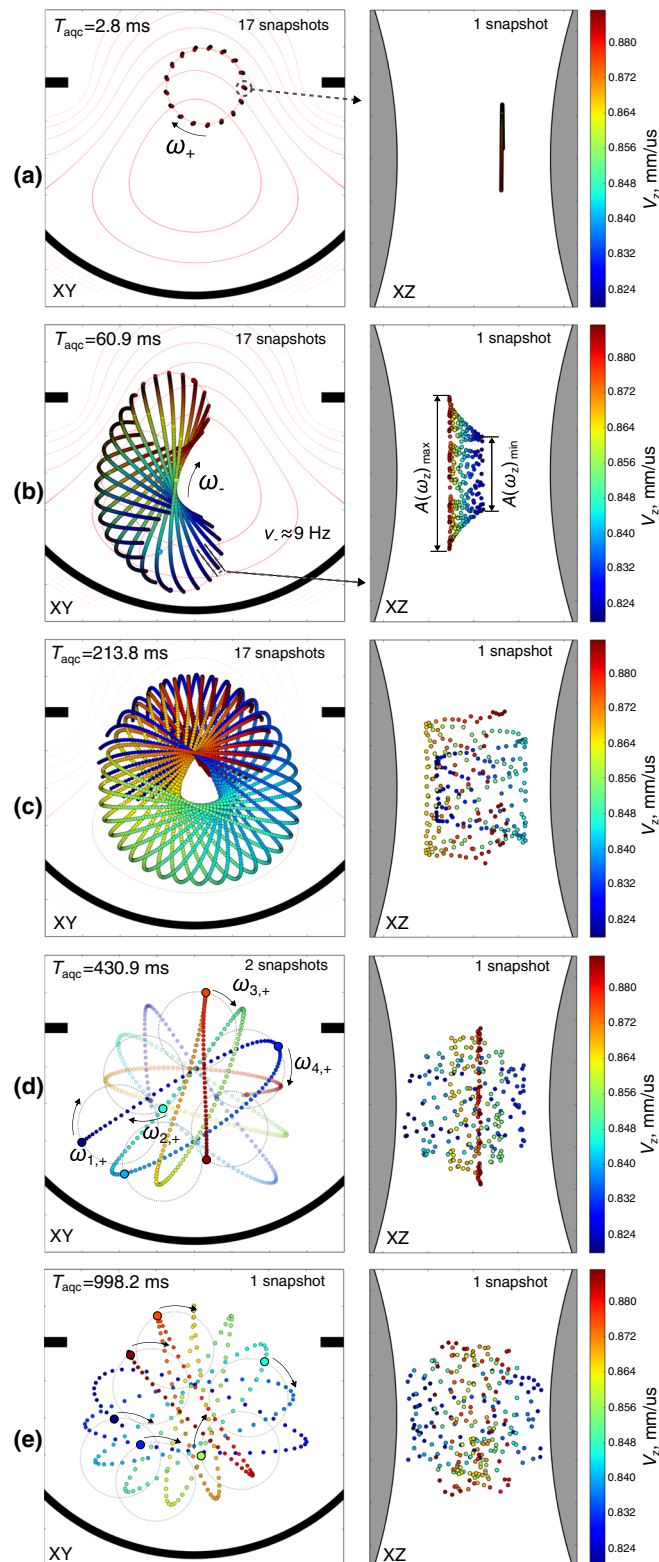
Figure 4. Snapshots of 2D projections of ion trajectories in the whole volume of a NADEL ICR cell at the specified acquisition periods onto the XY plane perpendicular and the XZ plane aligned with the magnetic field axis. The following acquisition periods, T_{acq}, are shown by panels: **(a)** – 2.8 ms, **(b)** – 60.9 ms, **(c)** – 213.8 ms, **(d)** – 430.9 ms, and **(e)** – 998.2 ms. Each ion was created with the predefined initial (pre-excitation) ion velocity V_z: $V_z = 0.82000 + 0.00025*n$ mm/us, where n = 0…279 (280 combinations in total). Initial ion coordinates: $z = 1$ mm; $x, y = 0.0$ mm. The corresponding parameters and transient generated by all ions with its frequency spectrum are as in Figure 3d

ICR cell onto the XY plane (Figure 4, left column) perpendicular and the XZ plane (Figure 4, right column) aligned with the magnetic field were plotted simultaneously for all 280 ions at five moments of time during the detection period. The dynamics of ion motion corresponding to Figure 4 is visualized in Video S1 (Supplementary Information).

Immediately after the excitation, each ion rotates at a cyclotron orbit around the axis, which almost matches the geometric center of the cell, and henceforth it can be referred to as the cyclotron oscillator. More precisely, the axis of each cyclotron oscillator starts to radially drift away from the geometric center already during the ion injection and trapping because to the applied offset DC potentials. However, the offset of the cyclotron oscillator's axis is negligible for the first several ms, and ions are still located in the region of a homogeneous excitation field. It means that ions of different m/z values in a wide m/z range could be excited to similar post-excitation cyclotron radii with a typical frequency sweep of 5–10 ms length (for broadband ion excitation). Figure 4a right panel shows that the ion cloud is axially stretched already at 2.5 ms passed after the end of a 300 us ion excitation because of a spread of initial (pre-excitation) ion velocities, despite the same starting coordinates x, y, and z for each ion.

The initially grouped ensemble of separate ion cyclotron oscillators follows the equipotential lines with the magnetron (drift) motion, radially stretching with time along the magnetron orbit, Figure 4b. Here the ions of a higher pre-excitation velocity V_z are in the head of the stretched ensemble (XY plane) and have higher amplitudes of axial oscillation (XZ plane). The distribution of the trapping electric potential is highly non-quadratic for the NADEL ICR cell, and the radial component of electric field strongly depends both on the azimuthal coordinate and on the axial coordinate, increasing while moving radially and axially from the center of the cell. It is well known that the magnetron and reduced cyclotron frequencies depend linearly on the reciprocal radial component of the electric field [1]. The ions with a high initial axial velocity V_z are influenced by a higher radial component because of a higher amplitude of axial oscillations. They obtain slightly smaller reduced cyclotron and higher magnetron frequencies on average during the detection period compared with the ions with a low initial axial velocity V_z. That is why the ions of a higher pre-excitation velocity V_z appear in the head of the stretched ensemble in the direction of a magnetron motion.

The separate cyclotron oscillators spread out on the magnetron (drift) orbit closing the ring after ~200 ms after the end of the excitation event, Figure 4c. The time period required for the ions to close the ring is determined by the magnetron frequency and, thus, by the applied trapping potential. A single snapshot of a 2D projection of a whole ion ensemble onto the XY plane demonstrates that ions form an elliptical structure that has the same

direction of the rotation as cyclotron motion. The number of ellipses that are azimuthally offset relative to each other increases with time, gradually forming a multipoint "star"-like figure, Figure 4d and e. Therefore, a characteristic motion of an ion ensemble inside the NADEL ICR cell demonstrates phase decoherence of magnetron frequencies for each ion with different initial axial velocity. That is why the ω_+ peak is averaged out in the cyclotron regime in the NADEL ICR cell with the application of the offset DC potentials. At the same time, $\omega_c = \omega_+ + \omega_-$ peak is dominant, as shown above, demonstrating phase coherence of cyclotron frequencies for each ion with different initial axial velocities, at least within the considered ion velocity spread of 20%–30% and trapping potential of 5 V. A similar behavior of a spatial distribution of an ion ensemble inside the NADEL ICR cell with the application of offset DC potentials was observed with simulations for a higher number of ions (500 ions), diverse trapping potentials (2.5 and 5 V), and Gaussian distributions of the initial parameters, including x, y, and z coordinates, Figure S3 (Supplementary Information). The simulations show that with an increase of the trapping potential the number of the ellipses increases and they become narrower.

Ion Cloud Structures in NADEL ICR Cells

Figures 5 and 6 demonstrate ion cloud structures for ion motion in the NADEL ICR cells with dipolar and quadrupolar ion detection, correspondingly. The difference between the panels in each figure is in the relation between the cyclotron and magnetron radii. When the ion magnetron radius is less than the cyclotron one, an ellipse (or an elliptical cylinder in a 3D space) is formed after ion spatial redistribution during 1 s ion detection, Figures 5 and 6 left panels. In a special case when the magnetron radius is equal to the cyclotron radius, ion slabs are formed, Figures 5 and 6 middle panels. A detailed consideration of the slab structure actually shows a very narrow elliptic cylinder structure. Finally, when the magnetron radius exceeds the cyclotron one, a tendency to form elliptic cylinders prevails again, Figures 5 and 6 right panels. As shown above in Figure 4 and Figure S3 (Supplementary Information), a number of elliptic cylinders can be formed, generating a star-like ion structure, Figure 5 right panel. Ion motion details revealed by SIMION indicate that either elliptic cylinders or slabs appear rotating at a Larmor (half cyclotron) frequency, whereas each ion oscillates along these ion structures. For example, in case of an ion slab formation, each ion goes through the center of the slab (the slab center coincides with the ICR cell center for the NADEL ICR cell with a quadrupolar ion detection), and fluctuates between this center and the poles (ends) of the slab, but each ion oscillates in its region of the cell, Video S2 (Supplementary Information). The reason for the slab rotation at the Larmor frequency is discussed below.
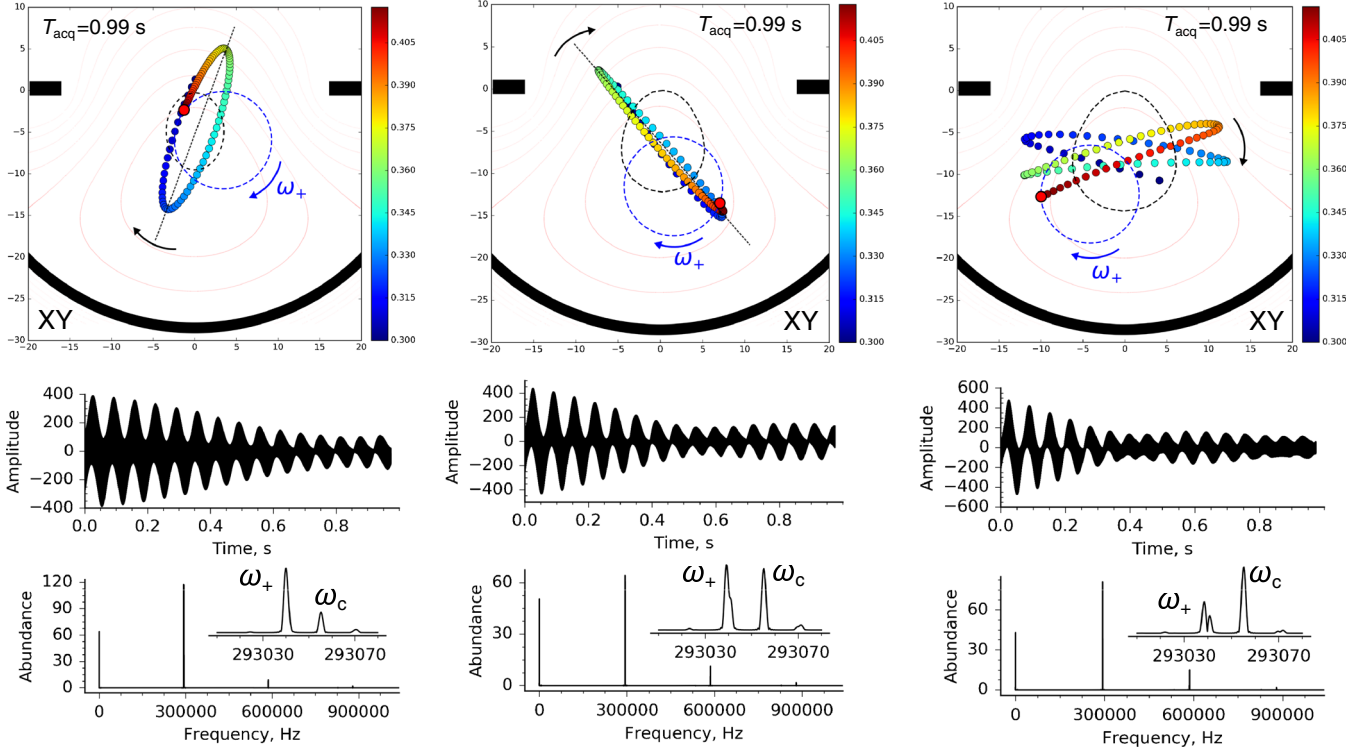
Figure 5. Ion cloud structures, corresponding transients, and frequency spectra generated by 100 ions (524 *m/z*) simulated during 1 s ion motion in the NADEL ICR cell with dipolar ion detection as a function of a ratio of cyclotron ($R_{cyclotron}$) to magnetron ($R_{magnetron}$) radii: (left panel) elliptic cylinder is formed when $R_{cyclotron} > R_{magnetron}$; (middle panel) slab is formed when $R_{cyclotron} \approx R_{magnetron}$, and (right panel) a complex start-like structure made of slabs and elliptic cylinders is formed when $R_{cyclotron} < R_{magnetron}$. Notice the intensities of the true and the reduced cyclotron frequency peaks. The following settings were employed for simulations: (left panel) $V_{E2} = 50$ mV; (middle panel) $V_{E2} = 100$ mV; and (right panel) $V_{E2} = 150$ mV. Other settings included $V_{trap} = 5$ V and $V_{E1} = -90$ mV employed for all panel. Each ion was created with an initial (pre-excitation) ion velocity V_z: $V_z = 0.3000 + 0.0011*n$ mm/us, where n = 0…99 (100 combinations in total). Ions were generated in the cell center, z = 70 mm and x, y = 0 mm, and immediately confined with trapping potential of 5 V applied to both trapping rings (no gated trapping)

An Analytical Model for Ion Slab Formation and Rotation

Let us consider a simplified model for ion motion in an ICR cell in which a standard quadratic trapping potential (without dependence on the azimuthal coordinate) is realized. The classical FT-ICR MS theory provides solutions for the frequencies of ion motion given by a reduced cyclotron frequency $\omega_+ = \frac{\omega_c}{2} + \sqrt{\left(\frac{\omega_c}{2}\right)^2 - \left(\frac{\omega_z}{2}\right)^2}$ and a magnetron frequency $\omega_- = \frac{\omega_c}{2} - \sqrt{\left(\frac{\omega_c}{2}\right)^2 - \left(\frac{\omega_z}{2}\right)^2}$, where ω_z is an axial oscillations frequency [1]. Subtracting one frequency from another produces a parametric frequency, ω_p: $\omega_+ - \omega_- = \omega_p = 2\sqrt{\left(\frac{\omega_c}{2}\right)^2 - \left(\frac{\omega_z}{2}\right)^2}$, or $\sqrt{\left(\frac{\omega_c}{2}\right)^2 - \left(\frac{\omega_z}{2}\right)^2} = \frac{\omega_p}{2}$. Solutions to the ion motion equation in a linear trapping field (quadratic trapping potential) of an ICR cell can be represented as a superposition of a cyclotron and magnetron phasors $|\tilde{r}| = |r_+ e^{-i\omega_+ t} + r_- e^{-i\omega_- t}|$, considered in the coordinate system originated at the axis of the ICR cell [29]. Under these conditions, consider a case when the cyclotron and mag-

netron radii are equal, $|r_+| = |r_-| = r = const$. The radius-vector for a single ion moving inside of an ICR cell would be thus given by:

$$\tilde{r} = r_+ e^{-i\omega_+ t} + r_- e^{-i\omega_- t} = r\left(e^{-i\omega_+ t} + e^{-i\omega_- t}\right)$$
$$= r \cdot e^{-i\frac{\omega_c}{2}t}\left(e^{-i\frac{\omega_p}{2}t} + e^{i\frac{\omega_p}{2}t}\right) = 2r \cdot e^{-i\frac{\omega_c}{2}t} \cdot \cos\frac{\omega_p}{2}t$$

In the equation above, $\frac{\omega_p}{2} = \frac{\omega_+ - \omega_-}{2} = \frac{\omega_c - 2\omega_-}{2} = \frac{\omega_c}{2} - \omega_- = \omega_{Larmor} - \omega_-$, where ω_{Larmor} denotes the Larmor frequency (a half of the cyclotron frequency). Therefore, the real part of a complex radius-vector describing ion motion is given by: $\mathrm{Re}\tilde{r}(t) = 2r \cdot \cos\frac{\omega_c}{2}t \cdot \cos\frac{\omega_p}{2}t = 2r \cdot \cos\omega_{Larmor}t \cdot \cos\frac{\omega_{Larmor} - \omega_-}{2}t$. In this equation, the first harmonic term describes vector (2D projection of a slab) rotation with a Larmor frequency, and the second harmonic term describes ion motion along the vector (a projection of the slab).

For a group of ions moving in an ICR cell upon ion detection, the summed radius-vector for motion of an ensemble of
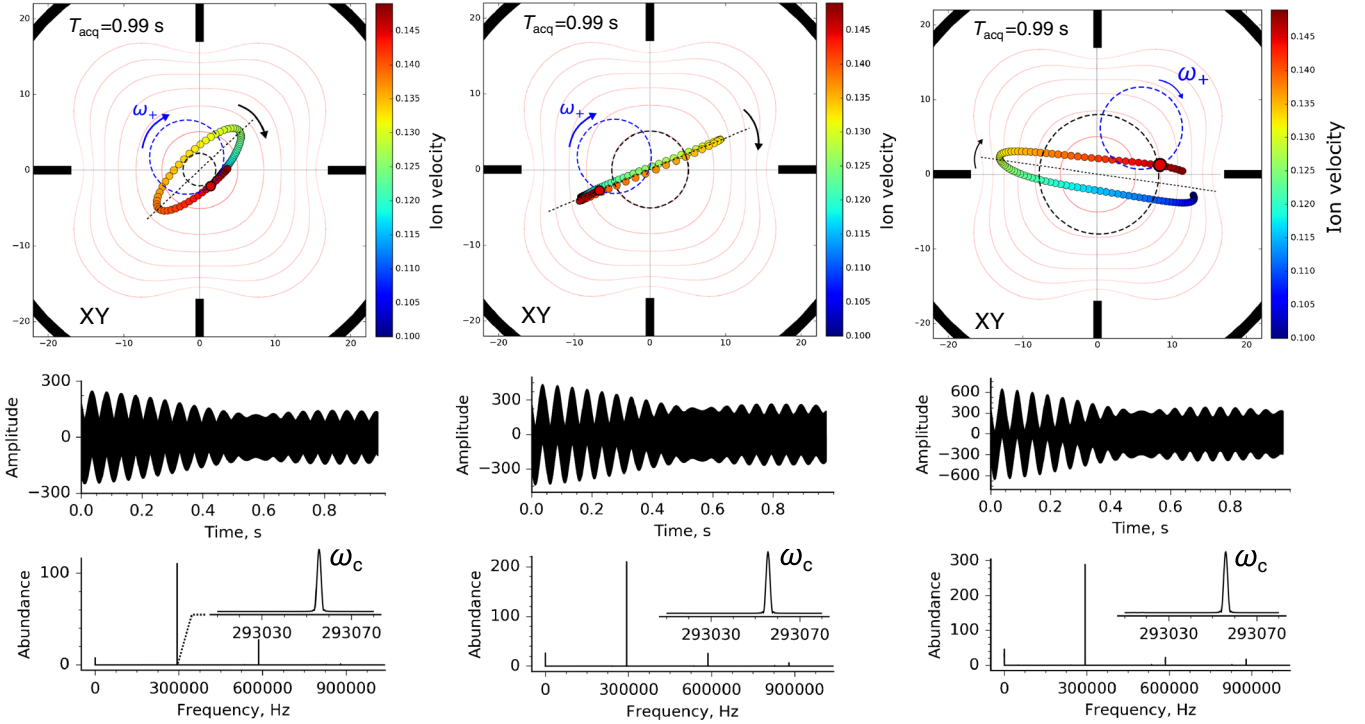
Figure 6. Ion cloud structures, corresponding transients, and frequency spectra generated by 100 ions (524 m/z) simulated during 1 s ion motion in the NADEL ICR cell with quadrupolar ion detection as a function of a ratio of cyclotron ($R_{cyclotron}$) to magnetron ($R_{magnetron}$) radii: (left panel) elliptic cylinder is formed when $R_{cyclotron} > R_{magnetron}$; (middle panel) slab is formed when $R_{cyclotron} \approx R_{magnetron}$, and (right panel) elliptic cylinders are formed when $R_{cyclotron} < R_{magnetron}$. Note the abundances of the true cyclotron frequency and the second harmonic of the reduced cyclotron frequency peaks. Each ion was created with the predefined initial (pre-excitation) ion velocity V_z: $V_z = 0.1000 + 0.0005*n$ mm/us, where $n = 0\dots99$ (100 combinations in total). Ions were generated in the cell center, $z = 70$ mm and $x, y = 0$ mm, and confined with a trapping potential of 5 V. The ion cyclotron motion was first excited by using sweep dipolar excitation. Then, ions were shifted from the cell center on a new magnetron orbit via the application of a DC pulse of $+/- 17$ V during a short time period $T_{sidekick}$: (left panel) $T_{sidekick} = 100$ us; (middle panel) $T_{sidekick} = 200$ us; and (right panel) $T_{sidekick} = 300$ us

ions is given by: $\tilde{R}(t) = \sum_k 2r \cdot e^{-i\frac{\omega_c}{2}t} \cdot \cos\left(\frac{\omega_{Larmor} - \omega_-^k}{2}t + \phi_{0k}\right)$, where $k = 1, 2, 3$, etc. When $t = 0$, the initial condition is described as $\tilde{R}(t = 0) = \sum_k 2r \cdot \cos(\phi_{0k})$. Therefore, the radii-vectors of ions in the cell are in phase for their cyclotron motion, but they have different phases for their magnetron motion because of the dispersion in the drift (magnetron) frequencies after the excitation, accounted for by the ω_-^k term, and the different initial phases ϕ_{0k}. The ion-specific value of ω_-^k indicates the dispersion in the magnetron (drift) frequencies due to the difference in the ion initial energies, which modulates ion axial oscillations and, in turn, varies the magnetron frequency. In the case of an ideal quadratic potential, the dispersion of the magnetron frequency is absent; however, when non-quadratic components are introduced, as in the case of NADEL ICR cells, this dispersion may become pronounced.

To visualize formation of the ion slab and its rotation according to the simplified analytical description given here, we can use the following equations to describe ion motion in a radial plane perpendicular to the magnetic field:

$$x_k(t) = 2r \cdot \cos\omega_{Larmor}t \cdot \cos\left(\frac{\omega_{Larmor} - \omega_-^k}{2}t + \phi_{0k}\right)$$

$$y_k(t) = -2r \cdot \sin\omega_{Larmor}t \cdot \cos\left(\frac{\omega_{Larmor} - \omega_-^k}{2}t + \phi_{0k}\right)$$

Numeric solutions of these equations of ion motion for typical parameters are presented in Video S3 (Supplemental Information). The obtained results rationalize slab rotation at the Larmor frequency and validate the basis of the unified model described below (see Figure 7). In line with the SIMION results, when the cyclotron and magnetron radii are equal, ions appear on a single line (which is a 2D projection from an ion slab in a 3D space). This line rotates at a Larmor (half-cyclotron) frequency about its axis. Each ion k moves back and forth along the line between its poles with a reduced Larmor frequency $(\omega_{Larmor} - \omega_-^k)$. Initial phase and initial magnetron frequency of each ion determine its position on the line at each moment in time. A group of ions may fill the line closer to evenly as a function of their initial parameters.
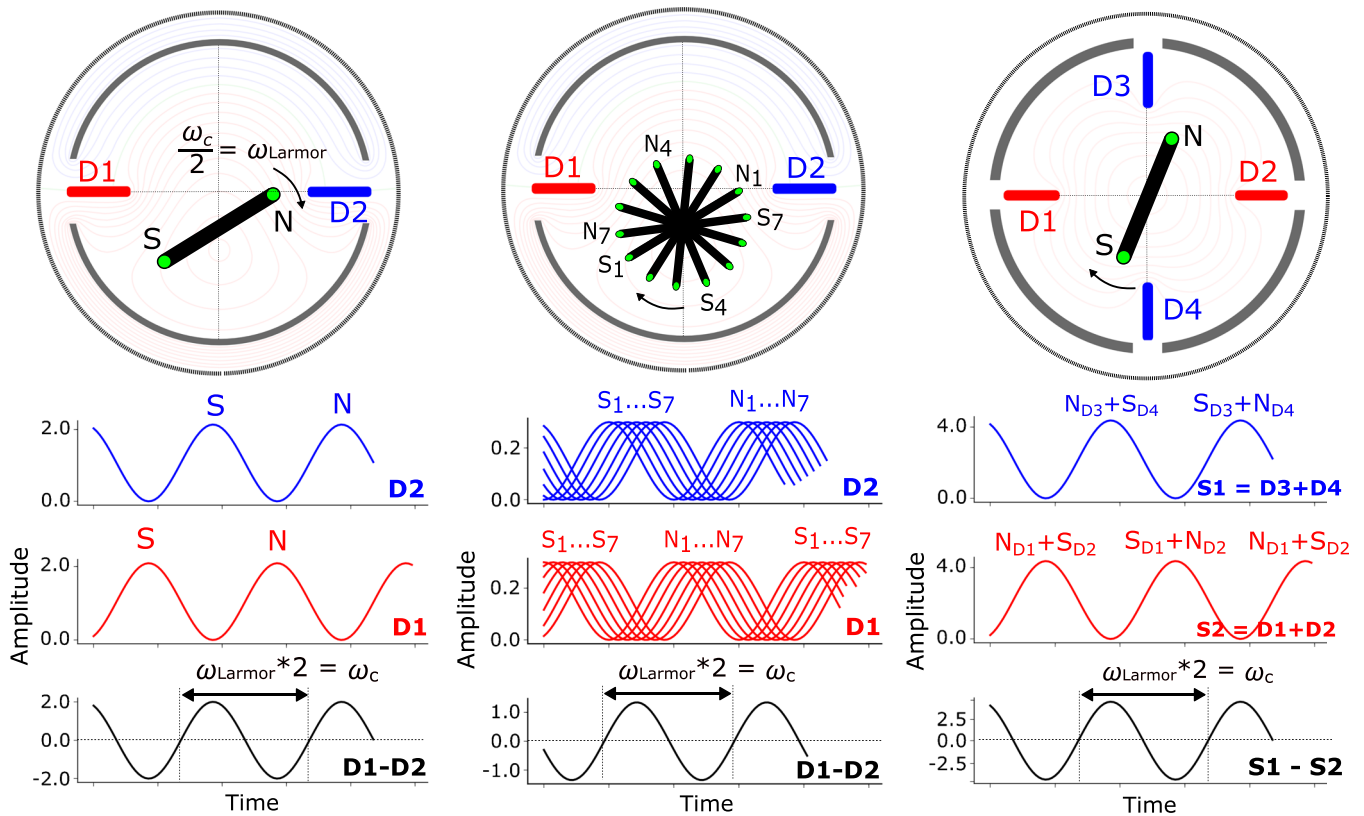
Figure 7. A unified model for the true cyclotron frequency generation in the NADEL ICR cells. The schematic representation of a time domain signal generation at the dominant true cyclotron frequency in the NADEL ICR cells (left and middle panels) with two detection electrodes and dipolar ion detection resulting in formation of a single slab and star-like configurations, and (right panel) with four detection electrodes and quadrupolar ion detection when a single slab configuration is realized. Slabs rotate at a half cyclotron frequency (the Larmor frequency) for all cases shown

In the non-linear trapping field of the NADEL ICR cells, the idealistic description given above induces a divergence from a thin slab into a thicker one, formed by the narrow elliptic cylinders, Figures 5 and 6, Video S2 (Supplemental Information). This transformation is manifested by the corresponding transient modulation. In the case when the cyclotron and magnetron radii are not equal, $|r_+| \neq |r_-|$, the slab will further transform into even more pronounced elliptic cylinders, Figures 5 and 6. Formation of a number of slabs, i.e., generation of a star-like ion structure, is directed, possibly, by a strong azimuthal dependence of the trapping potential (super-ellipse equipotential lines) when the magnetron radius exceeds the cyclotron radius in a highly non-linear trapping field.

A Unified Model of a Cyclotron Frequency Generation in NADEL ICR Cells

Based on the results presented above, we are now in a position to formulate a unified model for the true cyclotron frequency regime generation in FT-ICR MS, Figure 7. The main aspect of this model is the consideration of an ion slab rotating at a Larmor (half-cyclotron) frequency as a basic element of an organized ion motion, Video S3 (Supplemental Information). Induced current ion signal detection can then be performed by an appropriate arrangement of a given number of detection electrodes around the rotating ion slab. Interestingly, even a single

narrow aperture detection electrode would record a periodic signal at the cyclotron frequency from an ion slab rotating at the Larmor frequency, Figure 7 left panel. That is attributable to the signal maxima generation by the two ends of the ion slab – its North (N) and South (S) poles.

Historically, the distribution of ions into the slabs has been first suggested for the NADEL ICR cells with a quadrupolar ion detection in the case when magnetron and cyclotron radii are equal, Figure 7 right panel. This hypothesis was made owing not only to the SIMION simulations but, even more evidently, to the particle-in-cell (PIC) simulations (which allowed simulating motion of a larger number of ions at a time) performed in our collaboration with Amster's group [30]. Originally, the main attention of PIC simulations was put on the nature of a quadrupolar ion detection enabling FT-ICR MS operation at the cyclotron frequency. However, with the ion slab approach in hands for the quadrupolar ion detection, it became clear that it may also be the key toward a more general cyclotron frequency generation in the NADEL ICR cell, including for dipolar ion excitation and detection.

In the case of a NADEL ICR cell with a dipolar ion detection, signals from the two detection electrodes are subtracted. A single ion slab may be formed when cyclotron and magnetron radii are equal, Figure 7 left panel. It would provide a detectable signal only if the center of the slab is not on the same line with the two detection electrodes, but shifted up or down from the cell central axis. That is

exactly the case of ion cyclotron frequency generation with the NADEL ICR cell, as depicted in Figures 2 and 4. Indeed, the DC offset potentials are selected to maximize the intensity of the cyclotron frequency peak. However, it is also evident from Figure 5 middle panel that a single slab is not sufficient to eliminate the reduced cyclotron frequency component. As suggested by SIMION results in Figure 4 and Figure S3 (Supplemental Information), several slabs are to be formed to yield frequency (mass) spectra with preferentially cyclotron frequency peaks. More precisely, Figure 4 and Figure S3 (Supplementary Information) suggest that for the employed simulation parameters a star-like ion structure can be formed from seven slabs, the poles of which correspond to the poles of the star. Interestingly, as depicted in Figure 7 middle panel, increasing the number of slabs in the dipolar ion detection scheme leads to detection of a number of phase-shifted periodic ion signals at the true cyclotron frequency. Subtraction of the two periodic signals recorded by the two detection electrodes yields the final, slightly less intense but periodic signal, which also occurs at the cyclotron frequency.

Therefore, we conclude that the preferential cyclotron frequency generation in the NADEL ICR cell with dipolar ion excitation and detection takes place when a number of ion slabs (elliptic cylinders) form an ion star that rotates around its off-center axis at a Larmor frequency. The number of slabs is increased with detection time (with the number of magnetron periods of an ion cloud) and is also defined by the experimental parameters, e.g., the trapping voltage and distribution (azimuthal dependence), the initial ion velocities spread, and the ratio of cyclotron and magnetron radii. Increasing the number of slabs for a single m/z value leads to an overall signal decrease and thus is to be avoided. Reducing the number of slabs, toward 1–2 slabs for a single m/z value, increases the reduced cyclotron frequency component, which is undesirable. Therefore, about 7–10 slabs for a single m/z value is perhaps the upper limit, and 3–5 slabs is the lower limit for the star formation.

Conclusions

Ion motion simulations presented here suggest that upon ion detection in the NADEL ICR cells with a highly non-quadratic trapping potential, ion cyclotron oscillators do not form a cloud tightly bunched on the radial plane orthogonal to the magnetic field, but are spatially distributed in this plane and in the cell volume. The cyclotron motions for all ions in the ICR cell are in phase, whereas their magnetron (drift) frequencies and initial phases may differ significantly. The magnetron frequency and phase dispersions destroy frequency peaks that contain a magnetron frequency component: reduced cyclotron frequency, ω_+, peaks for dipolar ion detection, and $2\omega_+$ peaks for quadrupolar ion detection. At the same time, all ions in-phase contribute to the intensity of the cyclotron frequency, ω_c, peak.

Interestingly, SIMION simulations demonstrated that ion spatial redistribution in the NADEL ICR cells during ion detection in the non-quadratic trapping potential is not random, but forms fundamentally new types of ordered ion structures – elliptic cylinders and ion slabs, or their combination giving rise to the star-like structures. These ion structures rotate about their axes with a half cyclotron (Larmor) frequency as a whole, whereas each of the ions contributing to this motion appears as oscillating along these structures with a Larmor frequency reduced by the magnetron (drift) frequency. Consideration of these ion structures provides an alternative and visually enhanced explanation for the occurrence of FT-ICR MS at the cyclotron frequency.

The here presented initial insights into the understanding of the underlying mechanism of the cyclotron frequency regime in FT-ICR MS lights up the way for further rational design of ICR cells potentially leading to an improved performance of FT-ICR MS at the cyclotron frequency and further advances in its applications. Further insights into the performance characteristics of the NADEL ICR cells with cyclotron frequency detection, specifically approach sensitivity versus the "gold standard" ion cloud motion in FT-ICR MS, could be gained through ion motion simulations. A comprehensive analytical theory of ion motion in crossed magnetic and highly non-linear electric fields is required to reveal the minor details of the cyclotron frequency generation process.

Acknowledgments

References

1. Marshall, A.G., Hendrickson, C.L., Jackson, G.S.: Fourier transform ion cyclotron resonance mass spectrometry: a primer. Mass Spectrom. Rev. **17**, 1–35 (1998)
2. Amster, I.J.: Fourier transform mass spectrometry. J. Mass Spectrom. **31**, 1325–1337 (1996)
3. Nikolaev, E.N., Heeren, R.M.A., Popov, A.M., Pozdneev, A.V., Chingin, K.S.: Realistic modeling of ion cloud motion in a Fourier transform ion cyclotron resonance cell by use of a particle-in-cell approach. Rapid Commun. Mass Spectrom. **21**, 3527–3546 (2007)
4. Easterling, M.L., Mize, T.H., Amster, I.J.: Routine part-per-million mass accuracy for high-mass ions: space-charge effects in MALDI FT-ICR. Anal. Chem. **71**, 624–632 (1999)
5. Taylor, P.K., Amster, I.J.: Space charge effects on mass accuracy for multiply charged ions in ESI-FTICR. Int. J. Mass Spectrom. **222**, 351–361 (2003)
6. Schweikhard, L.: Theory of quadrupole detection Fourier transform ion cyclotron resonance. Int. J. Mass Spectrom. Ion Process. **107**, 281–292 (1991)
7. Schweikhard, L., Lindinger, M., Kluge, H.J.: Quadrupole-detection FT-ICR mass spectrometry. Int. J. Mass Spectrom. Ion Process. **98**, 25–33 (1990)
8. Heck, M., Blaum, K., Cakirli, R.B., Rodríguez, D., Schweikhard, L., Stahl, S.: Dipolar and quadrupolar detection using an FT-ICR MS setup at the MPIK Heidelberg. Hyperfine Interact. **199**, 347–355 (2011)
9. Chen, R., Guan, S., Marshall, A.G.: Generation and detection of coherent magnetron motion in Fourier transform ion cyclotron resonance mass spectrometry. J. Chem. Phys. **100**, 2258–2266 (1994)
10. Gabrielse, G.: The true cyclotron frequency for particles and ions in a Penning trap. Int. J. Mass Spectrom. **279**, 107–112 (2009)

11. Gabrielse, G.: Why is sideband mass spectrometry possible with ions in a Penning trap? Phys. Rev. Lett. **102**, (2009)
12. Ledford, E.B., Rempel, D.L., Gross, M.L.: Space charge effects in Fourier transform mass spectrometry. II. Mass calibration. Anal. Chem. **56**, 2744–2748 (1984)
13. Gorshkov, M.V., Good, D.M., Lyutvinskiy, Y., Yang, H., Zubarev, R.A.: Calibration function for the Orbitrap FTMS accounting for the space charge effect. J. Am. Soc. Mass Spectrom. **21**, 1846–1851 (2010)
14. Masselon, C., Tolmachev, A.V., Anderson, G.A., Harkewicz, R., Smith, R.D.: Mass measurement errors caused by "local" frequency perturbations in FTICR mass spectrometry. J. Am. Soc. Mass Spectrom. **13**, 99–106 (2002)
15. Smith, D.F., Kharchenko, A., Konijnenburg, M., Klinkert, I., Paša-Tolić, L., Heeren, R.A.: Advanced mass calibration and visualization for FT-ICR mass spectrometry imaging. J. Am. Soc. Mass Spectrom. **23**, 1865–1872 (2012)
16. Zubarev, R.A., Horn, D.M., Fridriksson, E.K., Kelleher, N.L., Kruger, N.A., Lewis, M.A.: Electron capture dissociation for structural characterization of multiply charged protein cations. Anal. Chem. **72**, 563–573 (2000)
17. Fung, Y.M.E., Adams, C.M., Zubarev, R.A.: Electron ionization dissociation of singly and multiply charged peptides. J. Am. Chem. Soc. **131**, 9977–9985 (2009)
18. Zhurov, K.O., Fornelli, L., Wodrich, M.D., Laskay, U.A., Tsybin, Y.O.: Principles of electron capture and transfer dissociation mass spectrometry applied to peptide and protein structure analysis. Chem. Soc. Rev. **42**, 5014–5030 (2013)
19. Vorobyev, A., Zhurov, K.O., Laskay, Ü.A., Tsybin, Y.O.: On the use of electron capture rate constants to describe electron capture dissociation mass spectrometry of peptides. Eur. J. Mass Spectrom. **21**, 451–458 (2015)
20. Nagornov, K.O., Kozhinov, A.N., Tsybin, Y.O.: Fourier Transform ion cyclotron resonance mass spectrometry at the cyclotron frequency. J. Am. Soc. Mass Spectrom. **28**, 768–780 (2017)
21. Tsybin, Y.O., Nagornov, K.O., Kozhinov, A.N.: Novel mass analyzers for rapid high-performance FT-ICR MS. Proceedings of the 63rd American Society for Mass Spectrometry Conference on Mass Spectrometry and Allied Topics, 31 May - 4 June 2015, St. Louis, Missouri, USA
22. Scigelova, M., Hornshaw, M., Giannakopulos, A., Makarov, A.: Fourier transform mass spectrometry. Mol. Cell. Proteomics. **10**, M111.009431 (2011)
23. Nagornov, K.O., Kozhinov, A.N., Tsybin, O.Y., Tsybin, Y.O.: Ion trap with narrow aperture detection electrodes for Fourier transform ion cyclotron resonance mass spectrometry. J. Am. Soc. Mass Spectrom. **26**, 741–751 (2015)
24. Hendrickson, C.L., Beu, S.C., Blakney, G.T., Marshall, A.G.: SIMION modeling of ion image charge detection in Fourier transform ion cyclotron resonance mass spectrometry. Int. J. Mass Spectrom. **283**, 100–104 (2009)
25. Wilcox, B.E., Beu, S., Hendrickson, C.L., Marshall, A.G.: Corrections to the SIMION 7.0 ICR demo user program. ICR/Ion Trap Newsletter of the National High Magnetic Field Laboratory. **67**, 11 (2002)
26. Breitenfeldt, M., Baruah, S., Blaum, K., Herlert, A., Kretzschmar, M., Martinez, F.: The elliptical Penning trap: experimental investigations and simulations. Int. J. Mass Spectrom. **275**, 34–44 (2008)
27. Vartanian, V.H., Laude, D.A.: Motional averaging of ions for control of magnetron motion in Fourier transform ion cyclotron resonance open-geometry trapped-ion cells. Int. J. Mass Spectrom. **178**, 173–186 (1998)
28. Luebkemann, F., Wanczek, K.P.: Miniature ICR cells. Int. J. Mass Spectrom. **281**, 150–156 (2009)
29. Tsybin, O.Y., Tsybin, Y.O.: Time-dependent frequency of ion motion in Fourier transform mass spectrometry. Int. J. Mass Spectrom. **376**, 75–84 (2015)
30. Driver, J.A., Nagornov, K.O., Kozhinov, A.K., Tsybin, Y.O., Kharchenko, A., Amster, I.J.: Multiparticle simulations of quadrupolar ion detection in an ion cyclotron resonance cell with four narrow aperture detection electrodes. J. Am. Soc. Mass Spectrom. https://doi.org/10.1007/s13361-017-1817-6